European Journal of Radiology 118 (2019) 153–160

Contents lists available at ScienceDirect

European Journal of Radiology

journal homepage: www.elsevier.com/locate/ejrad

Research article

Metallic dental artifact reduction in computed tomography (Smart MAR): Improvement of image quality and diagnostic confidence in patients with suspected head and neck pathology and oral implants

Felix Feldhaus[a,*], Georg Böning[a], Martin Jonczyk[a], Johannes Kahn[a], Uli Fehrenbach[a], M. Maurer[b], D. Renz[c], Bernd Hamm[a], Florian Streitparth[d]

[a] Charité – Universitätsmedizin Berlin, corporate member of Freie Universität Berlin, Humboldt-Universität zu Berlin, and Berlin Institute of Health, Department of Radiology, Augustenburger Platz 1, 13353 Berlin, Germany
[b] Department of Diagnostic, Interventional and Pediatric Radiology, Inselspital, University of Bern, CH-3010 Bern, Switzerland
[c] Department of Radiology, University of Jena, Am Klinikum 1, 07747, Germany
[d] Department of Radiology, Ludwig-Maximilians-University, Marchioninistr. 15, 81377 München, Germany

ARTICLE INFO

Keywords:
Computer-assisted image processing
Artifacts
Neck
Squamous cell carcinoma

ABSTRACT

Purpose: We determined whether the Smart MAR metal artifact reduction tool - a three-stage, projection-based, post processing algorithm - improves subjective and objective image quality and diagnostic confidence in patients with dental artifacts and suspected head and neck pathology compared to standard adaptive statistical iterative reconstructions (ASIR V) alone.

Method: The study included 100 consecutive patients with nonremovable oral implants or dental fillings and suspected oropharyngeal cancer or abscess. CT raw data of a single-source multislice CT scanner were post-processed using ASIR V alone and with additional Smart MAR reconstruction. Image quality of baseline ASIR V and Smart MAR-based reconstruction series was compared both quantitatively (5 regions of interest, ROIs) and qualitatively (two independent raters).

Results: Additional Smart MAR reconstruction significantly seems to improve both attenuation and noise adjacent to implants and in more distant areas (all $p < 0.001$) compared to standard ASIR V reconstructions alone. Signal-to-noise ratio (SNR; $p = 0.001$) and contrast-to-noise ratio were improved significantly (CNR; $p = 0.001$). Smart MAR improved visualization of tumor/abscess (detected in 36 of 100 patients, 36%) and representative oropharyngeal tissue ($p < 0.001$). In 8 of 36 patients (22%), tumor was only detected in Smart MAR series. Mean total DLP was 506.8mGy*cm; average CTDIvol was 5.5 mGy.

Conclusions: The supplementary use of the Smart MAR post-processing tool seems to significantly improve both subjective and objective image quality as well as diagnostic confidence and lesion detection in CT of the head and neck. In 22% of cases, the tumor was detected only in Smart MAR reconstructed images.

1. Introduction

Since the early days of computed tomography (CT), metal artifacts, including those caused by osteosynthetic or dental material, have reduced image quality and hence degraded the diagnostic yield of CT scans. Such artifacts are especially common in the oral cavity, where different types of metallic implants can cause a variety of surrounding artifacts and thus impair diagnostic accuracy by obscuring smaller soft tissue abnormalities such as tumors or inflammatory processes as well as bone invasion or erosion.

There are at least three important types of artifacts that can be caused by metal implants: beam hardening, photon starvation, and

Abbreviations: CNR, Contrast-to-noise ratio; CT, Computed tomography; CTDI, Computed tomography dose index; DE-CT, Dual-energy computed tomography; DLP, Dose-length product (in mGy*cm); HU, Hounsfield unit; IJV, Internal jugular vein; IQR, Interquartile range; MAR, Metal artifact reduction; MS-CT, Multislice computed tomography; ROI, Region of interest; SD, Standard deviation; SNR, Signal-to-noise ratio; SS-CT, Single-source computed tomography

* Corresponding author.
E-mail addresses: felix.feldhaus@charite.de (F. Feldhaus), georg.boening@charite.de (G. Böning), martin.jonczyk@charite.de (M. Jonczyk), johannes.kahn@charite.de (J. Kahn), uli.fehrenbach@charite.de (U. Fehrenbach), Martin.Maurer@insel.ch (M. Maurer), diane.renz@med.uni-jena.de (D. Renz), bernd.hamm@charite.de (B. Hamm), florian.streitparth@med.uni-muenchen.de (F. Streitparth).

https://doi.org/10.1016/j.ejrad.2019.07.015
Received 6 December 2018; Received in revised form 9 July 2019; Accepted 14 July 2019

scatter artifact [1].

Besides increasing tube current and lowering kV and peak voltage, metal-related artifacts can be reduced on conventional CT scanners to some extent by using different types of image reconstruction algorithms such as iterative and projection-based approaches [1–4] or dual-energy techniques [5–7]. Projection-based algorithms in patients with head and neck tumors report a significant reduction of metal artifacts and improved evaluation of head and neck soft tissues compared to iterative reconstructions alone [2,3,8,9].

The purpose of the present study was to investigate whether new metal artifact reduction software (Smart MAR) improves subjective and objective image quality and diagnostic confidence in patients with metallic oral implants undergoing head and neck CT for suspected pathology (new tumor, recurrent tumor after surgery, abscess) compared with standard adaptive statistical iterative reconstruction (ASIR V) alone.

2. Material and methods

2.1. Patients and study design

One hundred consecutive patients with metallic oral implants scheduled to undergo a clinically indicated CT scan for known or suspected head and neck pathology (tumor, abscess) were included in this prospective study. Patients were recruited consecutively from routine clinical cases of a single center over a period of six months (see Fig. 1). Eligibility criteria were 1) age of > 18 years, 2) clinical indication for a CT of head and neck, 3) presence of oral metal artifacts (caused by nonremovable prosthesis, screws, or dental fillings), and 4) CT protocol including postprocessing reconstruction with both Smart MAR and ASIR V. Exclusion criteria were 1) contraindication to CT and contrast agent administration (e.g., allergy to iodinated contrast agent, hyperthyroidism, impaired renal function with serum creatinine > 1.3 mg/dl).

Image quality of the Smart MAR-based reconstruction series was evaluated both quantitatively (in 5 regions of interest (ROIs) and qualitatively (two independent raters) and compared standard ASIR V.

The local ethics committee approved the study, and written informed consent was obtained.

2.2. CT scan parameters

All CT scans were acquired on a 64-row multislice CT scanner (MSCT; Revolution Evolution, GE Healthcare, Milwaukee, WI, USA) using a single-source x-ray tube with the following scan parameters: collimation 64 × 0.625 mm; rotation time 0.4 s; pitch 0.9; 120 kV; variable mAs adjusted to the patient's body mass index.

The head and neck scans were acquired after injection of 120 ml contrast agent (Ultravist 370, Bayer, Leverkusen, Germany) via the peripheral veins at a rate of 3 ml/s in split-bolus technique to achieve optimal contrast between soft tissues, tumor and of veins and arteries: First bolus of 80 ml (flow 3 ml/s; 27 s) followed by first saline flush (63 ml; 0.7 ml/s; 90 s), second bolus of 40 ml (3 ml/s; 13 s) after 120 s, and final saline flush (40 ml; 3 ml/s; 13 s). The head and neck scan was acquired 150 s after start of the first bolus injection.

2.3. CT image reconstruction

Standard adaptive iterative reconstruction (ASIR V, GE Healthcare, Milwaukee, WI, USA) was applied with identical settings in both reconstruction series. From the acquired CT raw data, the Smart MAR postprocessing tool (GE Healthcare, Milwaukee, WI, USA) automatically generates additional projection-based, reconstructed images in three steps: First, corrupted areas in the projection corresponding to metal are identified, and metal traces are segmented from the sinogram. Second, inpainted data are generated by interpolation and replace metal-corrupted projections where the metal sinogram is blended out. A corrected version is generated using forward projection of the classified

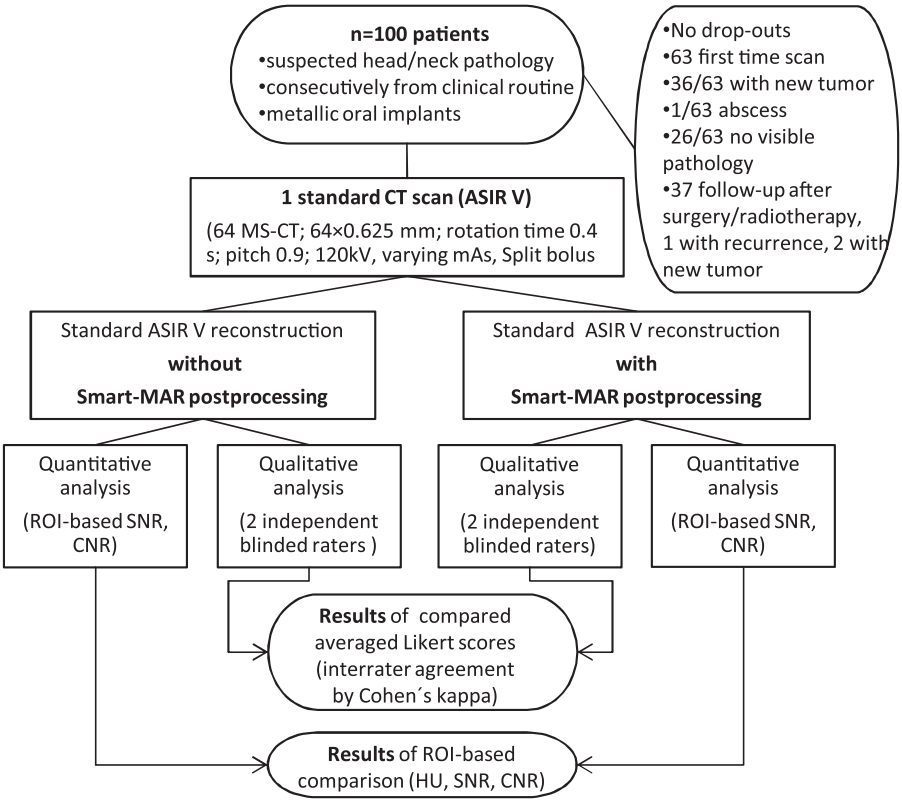

Fig. 1. Flow chart of study design.

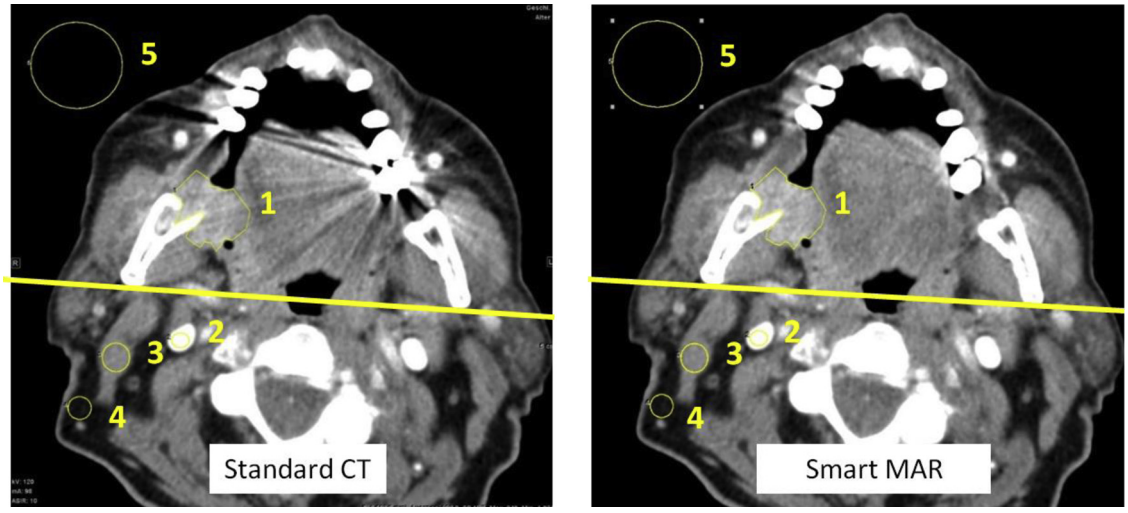

Fig. 2. Thin yellow lines outline the regions of interest (ROIs) placed for objective image analysis: ROI_1, (polygonal) area of tumor or, if no tumor apparent, area of tongue tissue; ROI_2, ipsilateral internal jugular vein; ROI_3, ipsilateral sternocleidomastoid muscle; ROI_4, fatty tissue; and ROI_5, surrounding air for measuring background noise. In both series, ROIs were as large as possible and were identical in shape and area. For subjective image evaluation by two readers using a Likert scale, axial slices were additionally divided into rostral and occipital areas (thick yellow line).

Table 1
Patient characteristics, CT findings, and radiation doses. A total of 100 CT scans of the head and neck were analyzed, including 63 examinations for suspected pathology or pretherapeutic workup and 37 follow-up examinations after surgery or radiation/chemotherapy. Official target values according to Bundesamt für Strahlenschutz, June 2016 [16].

Mean age (years)		67 (SD 4,2)
Male/female sex		67/33 (♀33%)
Detected tumors (including initial scans and follow up)		36 of 100 (36%)
Squamous cell cancer		32 (89%)
• Nasopharynx		3 (8%)
• Oropharynx		24 (67%)
• Hypopharynx		6 (17%)
Adenocarcinoma (1 submandibular gland, 2 thyroid gland)		3 (8%)
Abscess		1 (1% of all scans)
Follow-up examinations		37 of 100 (37%)
• Recurrence		1 (3% of follow ups)
• New tumor		2 (5% of follow ups)
• Initial tumor in oropharynx		27 (73%)
• Initial tumor in hypopharynx		7 (19%)
• Other initial tumor		3 (8%)
Detected tumors only in Smart MAR reconstructions		**8 of 36 tumors; 22%)**
Additonal MRI examination (number of cases)		
• In period of 8 weeks after CT scan		**7 (7%)**
• In period of 8 weeks before CT scan		**7 (7%)**
• Deviation MRI / CT report		**none**
Dose	Official target value, July 2016	**Mean (SD)**
CTDIvol head/neck [mGy]	15	**5.5** (SD 1.1)
CTDIvol thorax [mGy]	10	**8.5** (SD 1.3)
DLP total [mGy*cm]	680 (330 + 350)	**506.8** (SD 116.2)

image. In the third step, the final corrected projection is generated using both original projection data and the inpainted projections [10]. Projection-based algorithms from all known manufacturers appear to be based on similar mechanisms [9]. However, detailed information on the (validated) algorithms such as the exact interpolation method or projection thresholds is not available to users. For standard and additional Smart MAR series, thin (0.625 mm) and thick (3.75 mm) axial slices and 2.0 mm coronal and sagittal reconstructions were generated.

2.4. CT image analysis

Image quality of the routine ASIR V CT datasets (referred to as standard series) and additional Smart MAR reconstructions was evaluated quantitatively and qualitatively using our institution´s picture archiving and communication system (PACS) workstation (Centricity Radiology RA1000; GE Medical Systems).

2.5. Quantitative image analysis

The mean CT number (in Hounsfield units, HU) and standard deviation (SD (i.e., image noise) were recorded in circular ROIs. ROIs were placed in exactly the corresponding standard and Smart MAR series (3.75 mm slice thickness, Fig. 1) including an area of maximum streaking/beam hardening artifact within the particular structure with the assumption that this would best reflect the extent of metal artifact [8,11,12]: ROI_1, tumor or, if no tumor apparent, area of tongue; ROI_2, ipsilateral internal jugular vein (IJV); ROI_3, ipsilateral sternocleidomastoid muscle; ROI_4, fat; and ROI_5, surrounding air for noise. ROIs were as large as possible and identical in shape. $ROIs_{2\text{-}5}$ were positioned ipsilateral to the site of the tumor or metal implant. ROI_6 was drawn in the intraoral soft tissue within 1 cm distance from the implanted metal in the image subjectively most affected by artifacts.

Signal-to-noise ratio (SNR) was defined using the following formula: $SNR = ROI_1/SD_{ROI5}$. Contrast-to-noise ratios (CNRs) were calculated using following, established formula: $CNR = (ROI_1 - ROI_{2\ or\ 3}) / ROI_5$ (or background noise) [13,14]. CNRs were calculated for and IJV as well as tumor/tongue and sternocleidomastoid muscle, respectively.

2.6. Qualitative image analysis

Two radiologists (13 and 4 years of experience in reading head and neck CT scans), reviewed the two series of datasets independently, in random order and blinded to the presence of significant pathology (i.e., tumor or abscess) and information on patient history. The axial slices with the most severe artifacts were compared with the corresponding slices. Axial slices were evaluated in the soft tissue window, which could be adapted (standard level, 40; width, 350). Overall image quality was evaluated on a five-point Likert scale (see below). Furthermore, axial slices were divided into rostral and occipital areas by a line connecting the left and right occipital mandibular rami (see Fig. 2).

The following features were evaluated subjectively and independently: qualitative noise (ranging from 1 = unacceptable to 5 = minimal), soft tissue contrast (1 = very poor,…, 5 = excellent), visualization of small structures (1 = unacceptable,…, 5 = excellent),

Table 2
Nonparametric results of quantitative, ROI-based analysis in Hounsfield units (HU), median and interquartile range (IQR = third quartile (Q3) – first quartile (Q1)). P-values obtained by nonparametric Wilcoxon signed-rank test. ROI, region of interest; SD, standard deviation; SNR, signal-to-noise ratio; CNR, contrast-to-noise ratio. After Bonferroni correction of alpha level α` = 0.002, only p-values < 0.002 indicate statistically significant differences.

n = 100	Standard (ASIR V)	Smart MAR	*P* value
ROI_1 (tumor/tongue)	93, IQR 46	88, IQR 46	**0,001**
SD ROI_1 (tumor/tongue)	31, IQR 18	27, IQR 12	< **0.001**
ROI_2 (ipsilateral IJV)	254, IQR 96	253, IQR 100	**0.024**
SD ROI_2 (ipsilateral IJV)	18, IQR 8	18, IQR 6	0.118
ROI_3 (ipsilateral sternocleidomastoid muscle)	67, IQR 20	65, IQR 21	0.908
SD ROI_3 (ipsilateral sternocleidomastoid muscle)	13, IQR 5	12, IQR 4	**0.037**
SD ROI_4 (ipsilateral fat)	16, IQR 8	15, IQR 8	**0.031**
SD ROI_5 (air)	13, IQR 19	12, IQR 7	< **0.001**
HU ROI_6 (adjacent to artifact)	175, IQR 218	105, IQR 72	< **0.001**
SD HU ROI_6 (adjacent to artifact)	156, IQR 288	53, IQR 88	< **0.001**
SNR	7.4, IQR 7.6	7.9, IQR 6.2	**0.001**
CNR (air, IJV)	12.6, IQR 13.0	14.1, IQR 12.4	**0.001**
CNR (air, sternocleidomastoid muscle)	2.2, IQR 2.8	2.3, IQR 3.6	0.148

Table 3
Results of qualitative analysis by two readers using a 5-point Likert scale (1 worst, 5 best), results expressed both in mean ± standard deviation (SD) and median and interquartile range (ordinal scale, non-parametric; IQR = third quartile (Q3) - first quartile (Q1)). Results from non-parametric Wilcoxon signed-rank test. Values are means based on the ratings of both readers. Interrater agreement analyzed by Cohen´s kappa was κ > 0.56 for rostral regions and κ > 0.41 for occipital regions with a p-value of < 0.001 for both rostral and occipital regions.

N = 100	Standard (ASIR V)		Smart MAR		*p* value =
Noise	1.7 ± 0.6	2 IQR 1	2.8 ± 0.5	3 IQR 0.5	< **0.001**
Occipital	2.8 ± 0.5	3 IQR 0.5	3.8 ± 0.5	4 IQR 0.5	< **0.001**
Contrast	1.3 ± 0.5	1 IQR 0	2.6 ± 0.5	3 IQR 1	< **0.001**
Occipital	2.8 ± 0.6	3 IQR 1.4	3.8 ± 0.6	3 IQR 1.4	< **0.001**
Small structures	1.2 ± 0.6	1 IQR 0	2.5 ± 0.5	2.5 IQR 1	< **0.001**
Occipital	2.9 ± 0.6	3 IQR 0.5	3.9 ± 0.7	4 IQR 1	< **0.001**
Suspected lesion	1.4 ± 0.9	1 IQR 0	2.8 ± 0.8	3 IQR 1	< **0.001**
Occipital	3.1 ± 0.9	3 IQR 1.5	4.5 ± 0.6	4.5 IQR 1	< **0.001**
Artifacts	1.3 ± 0.8	1 IQR 0	2.5 ± 0.8	2 IQR 1	< **0.001**
Occipital	3.2 ± 0.8	3 IQR 0.9	4.4 ± 0.5	4.5 IQR 1	< **0.001**
Diagnostic confidence	1.5 ± 0.9	1 IQR 0.5	2.7 ± 0.9	2.5 IQR 1	< **0.001**
Occipital	3.9 ± 0.6	4 IQR 0	4.8 ± 0.4	5 IQR 0	< **0.001**

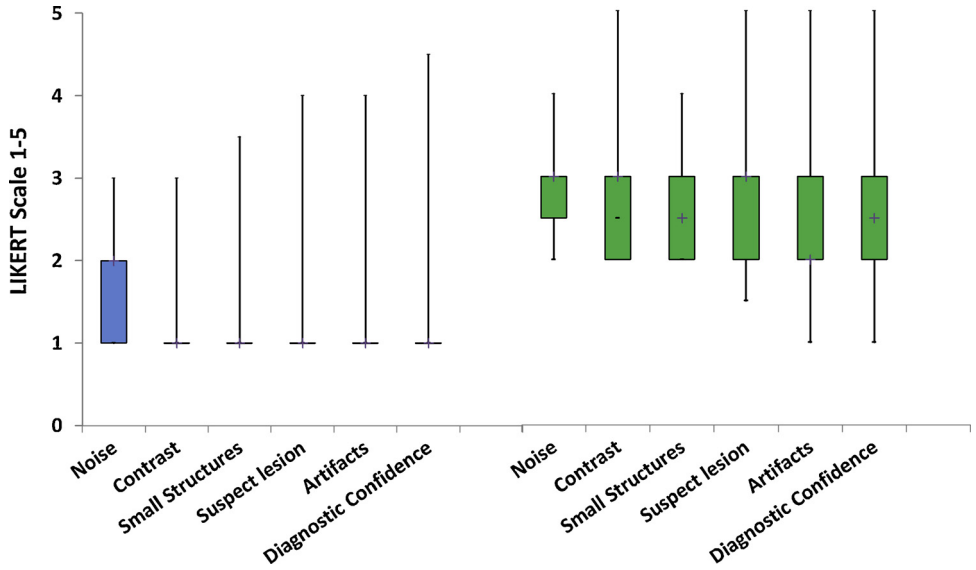

Fig. 3. Boxplot of the results of qualitative analysis using a 5-point Likert scale (1 worst, 5 best) for assessment of five parameters and overall diagnostic confidence. Median values, interquartile ranges (boxes), and ranges (whiskers) are snown. Blue: ratings for standard ASIR V datasets. Green: ratings for Smart MAR datasets.

visualization/delineation of suspicious lesions (1 = mimicking artifact, …, 5 = very conspicuous lesion with well-visualized margins), extent of artifacts (1 = major streak artifacts,…, 5 = no artifact) and diagnostic confidence, defined as improved lesion detection (1 = not confident,…, 5 = very confident). The distribution and volume of metal artifacts were evaluated subjectively using a four-point rating scale: 3 = extensive (> 75% bridges, multiple pin implants), 2 = moderate (25–75% implant bridges and/or > 5 pin.), 1 = minimal (< 25% implant bridge and/or < 5 pin implants) and 0 = no artifacts.

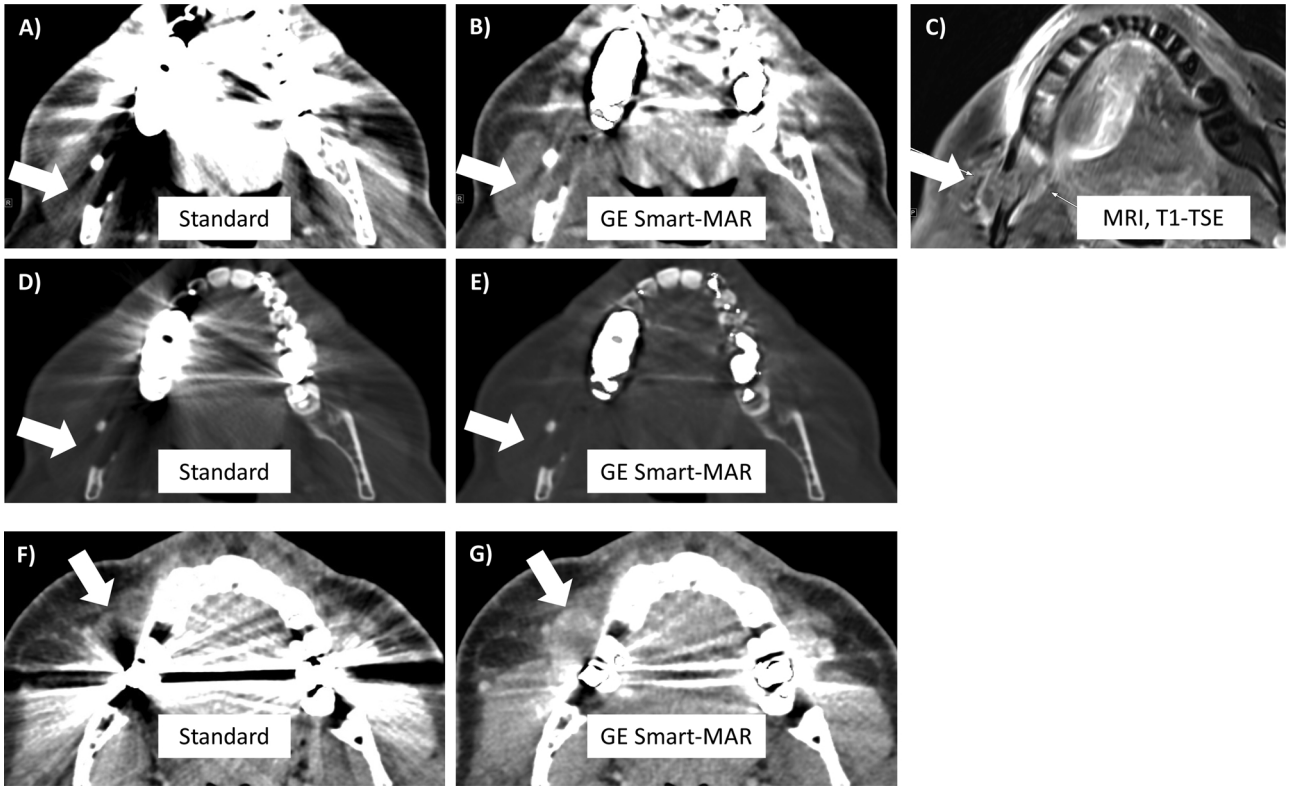

Fig. 4. Examples (SL, 3.75 mm; CE, 120 ml (split bolus 80/40 ml, 3 ml/s); soft tissue and bone window).
Example 1 (A–E): 38-year-old female, follow-up after tumor resection. Patient presenting with swelling, arrows indicate tumor mass. Histology: invasive SCC, TNM pT1 pN0 G2 R0 L0 V0. Arrows indicating tumor: A) tumor obscured in standard reconstruction, B) tumor unmasked in MAR images, C) MRI showing osteolytic tumor, (D,E) bone windows of same patient.
Example 2 (F, G): 68-year-old male, clinical suspicion of head and neck cancer. Arrows indicate enhancing tumor at the right mandible, not clearly visible in standard CT (F), but unmasked in MAR series (G). Histology: invasive SCC of right mandible, cT4a cN0 cM0 G2.

2.7. Dose analysis

Radiation doses in terms of dose-length products (DLP) and computed tomography dose indices (CTDIvol) were taken from dose protocols.

2.8. Statistical analysis

Statistical analysis was performed using SPSS 24.0 software (SPSS, Chicago, IL, USA). Nonparametric (tested by Shapiro Wilk test), continuous variables are provided as median +/- interquartile range (IQR). Differences in all objective image quality parameters (median and IQR) were analyzed using the nonparametric Wilcoxon signed-rank test. Subjective image quality was analyzed by averaging the two 5-point Likert scores and using the nonparametric Wilcoxon signed-rank test; results are provided both as mean +/- standard deviation (SD) and median and IQR [15]. Interrater agreement was analyzed by Cohen's kappa (κ) analysis (coefficient interpretation: κ: 0.21 − 0.40 = fair, 0.41 − 0.60 = moderate; 0.61 − 0.80 = substantial; κ: 0.81 − 1.0 = almost perfect agreement) [16]. A *p*-value less than 0.05 was considered to indicate a statistically significant difference.

The given alpha value ($\alpha = 0.05$) were adjusted using Bonferroni correction for multiple comparison of several (in our case n = 25) statistical tests. Multiple alpha ($\alpha`$) was set to $\alpha` = \alpha/25 = 0.002$ [17]. All p values are reported in the text are reported without Bonferroni correction.

3. Results

3.1. Patient data and scan parameters

The 100 study patients (67 male, 33 female) had a mean age of 67 (± 4.2) years. A tumor was identified in 36, an abscess in one of the 63 patients who underwent CT before treatment. The remaining 37 CT scans were follow-up examinations after surgery and/or radiochemotherapy and revealed recurrent tumor in one case (Fig. 4) and a new tumor in two patients (for details see Table 1).

The mean dose-length-product (DLP) of the entire scan (head and neck region and chest) was 506.8 mGy*cm; the average CT dose index (CTDIvol) was 5.5 mGy for the head and neck region.

3.2. Quantitative analysis

In axial reconstructions, ROI-based analysis showed the highest attenuation in ROI_6, directly adjacent to the most severe artifacts; noise was also highest in these regions (see Table 2). As mentioned above, multiple alpha was set to $\alpha` = \alpha/25 = 0.002$. Except for ROI_2, SD ROI_4 and SD ROI_3, p-values showed significant p-values even after adjustment of α-level. Both median attenuation and noise were significantly lower in the Smart MAR reconstructions (ROI_6: 175 HU, IQR 320-102 vs. 105, IQR 143-71 with MAR, $p < 0.001$). Comparison of the results for tumor or representative tongue tissue revealed significant differences with Smart MAR images showing lower attenuation and noise compared to ASIR V reconstructions (Table 2, ROI_1 /SD, p = 0.001). Significantly lower values for standard deviation were also found in ROI_5 (background noise) with $p < 0.001$. A statistically significant increase in SNR ($p = 0.001$, median of 7.4–7.9, SNR 6% higher with

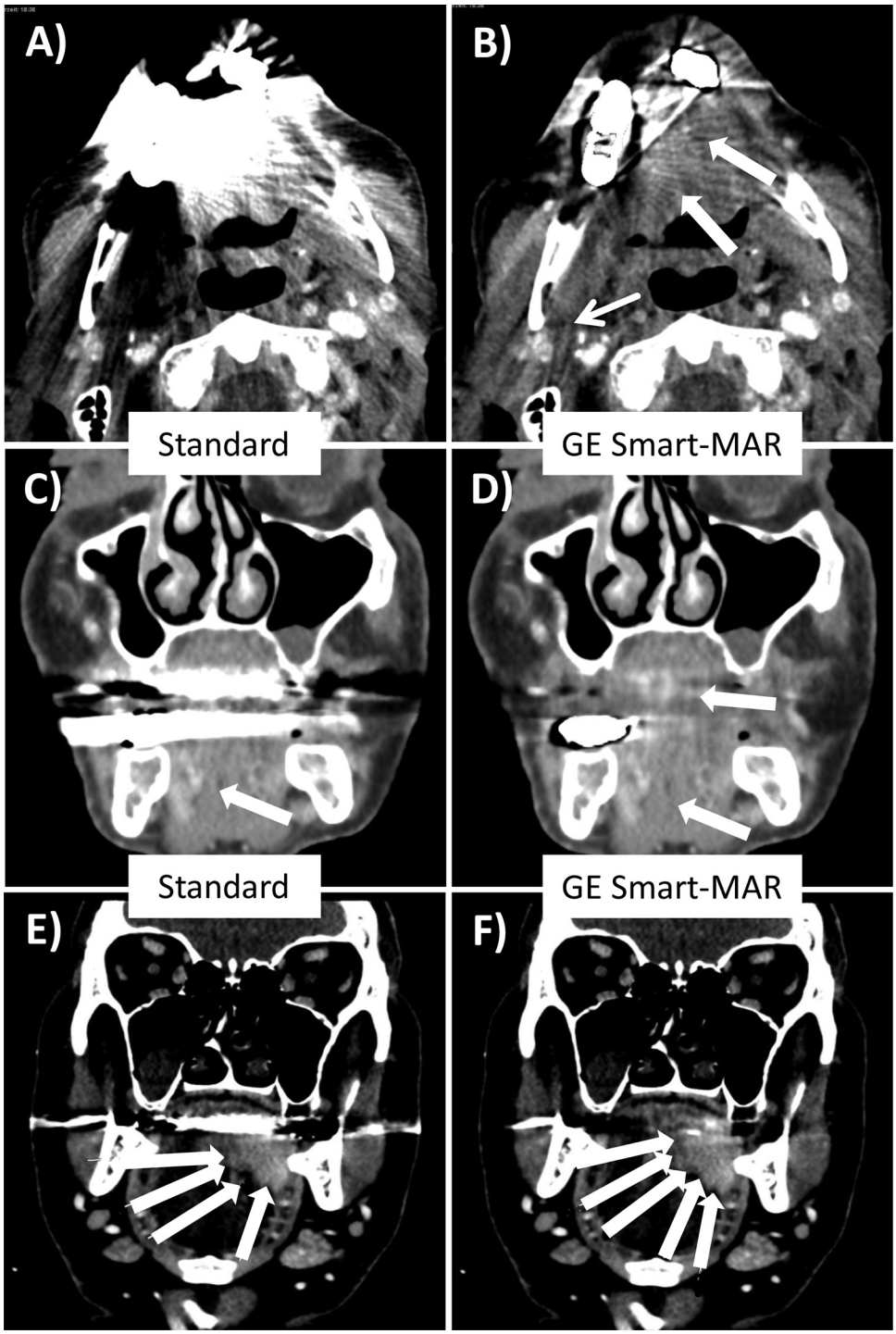

Fig. 5. Examples 3 and 4 (SL, 2.0 mm; CE, 120 ml (split bolus 80/40 ml, 3 ml/s); soft tissue kernel).
Fat arrows indicating tumor mass in both examples.
Example 3 (A–D): 76-year-old male, initial diagnosis of invasive SCC, pT2 pN0 G2 R0 L0 V0 G2, right lower mandible. Fat arrows indicating tumor mass both in axial and 2D reconstructions. In Smart MAR reconstructed images (B, D) image quality is still affected by persisting artifacts, but detection of tumor margins and evaluation of soft tissues as tongue or vessels (thin arrow) is improved.
Example 4 (E, F): 59-year-old male, initial diagnosis of invasive SCC, pT4a pN2b cM0 R0. Arrows indicate enhancing tumor mass, parts of tumor unmasked in MAR reconstructed image (F).

Smart MAR) and CNR including attenuation of IJV ($p = 0.001$, 11% increase) was detected. No difference was found for attenuation and standard deviation of ROI_3 and CNR including ROI_3 (sternocleidomastoid muscle).

3.3. Qualitative analysis

There was excellent interrater agreement regarding the assessment of the distribution and volume of implant artifacts (Cohen´s kappa, $\kappa = 0.9, p < 0.001$): n = 56 (Rater 1, 56%)/ n = 58 (Rater 2, 58%) with regard to extensive artifacts, n = 27 (Rater 1, 27%)/n = 25 (Rater 2, 25%) for moderate artifacts and n = 17 (for both raters, 17%) for minimal artifacts. The subjective evaluation of the artifacts differed only in 4 cases between the two raters. More than half of the scans were degraded by massive artifacts (56%/58%), 83% showing moderate to massive artifacts.

No rater found complete failure of Smart MAR or considerable induction of new artifacts. Regarding all six features assessed qualitatively using a Likert scale (noise, contrast, visualization of small structures and of tumor/tongue, extent of artifacts, and overall diagnostic confidence for ruling out/identifying lesions), the Smart MAR reconstructions received significantly higher ratings (all $p < 0.001$), even after correction of α level to $\alpha` = 0.002$ (see Table 3 und Fig. 3).

Even in the subgroup of 54 patients with high-grade artifacts, all six

items including diagnostic confidence were significantly improved by Smart MAR (all $p < 0.001$). In eight patients presenting with tumor/abscess in CT (22%), tumor was only detectable in the Smart MAR-reconstructed images, see examples presented in Figs. 4 and 5.

Interrater agreement, as assessed by Cohen's kappa, was moderate (for rostral areas adjacent to artifacts all $\kappa > 0.56$ versus $\kappa > 0.41$ for occipital areas; p-values < 0.001).

4. Discussion

The purpose of the present study was to investigate whether the new, commercially available Smart MAR tool, a projection-based metal artifact reduction algorithm, improves image quality and diagnostic confidence in patients with metallic oral implants undergoing CT scanning for suspected head and neck pathology.

Our results indicate that objective image quality parameters differ significantly for CT images reconstructed using Smart MAR in addition to standard (iterative) reconstruction. Attenuation and SD of tumor and adjacent soft tissues (as potential correlate of decreased artifacts and noise) were reduced. Furthermore, we found lower SD values for surrounding air as an indicator of reduced background noise (about 30% reduction). SNR and CNR seemed to benefit from Smart MAR application even after adjustment of alpha level.

The improvement of objective parameters of image quality is confirmed by studies of comparable projection-based MAR algorithms. O-MAR algorithm reduced noise, mean attenuation and SD or, as we could show it for Smart MAR in head and neck region, reduce streak artifacts in patients with orthopedic implants [11,18,19].

For evaluation of artifacts, however, these objective parameters should be interpreted with caution because lower median attenuation or standard deviation in ROIs as well as higher SNR/CNR are also consistent with heterogeneous artifacts (e.g., white and black streaks) adjacent to implants. For this reason, our objective results may simply indicate a different distribution of artifacts rather than improved image quality.

Nevertheless, the trends suggested by objective evaluation are supported by our subjective, rater-based results. All investigated parameters were rated higher after reconstruction using the Smart MAR algorithm ($p < 0.001$) in both rostral and occipital regions. Smart MAR significantly improved diagnostic confidence in areas adjacent to implants (1.5 SD 0.9–2.7 SD 0.9, $p < 0.001$). Even in a subgroup of 54 patients with the most extensive streak artifacts, ratings for Smart MAR reconstructions were significantly higher (all $p < 0.001$).

New MAR techniques are often compared with simple reconstruction algorithms [1], whereas ASIR V (our baseline reconstruction) is the newest reconstruction algorithm with excellent image quality [13,20]. Iterative or projection based reconstructions often yield superior image quality, but many studies were carried out only in phantoms or in CT for radiation planning [21–23].

The significant clinical value of Smart MAR reconstruction for head and neck CT is underlined by the fact that in our study in 22% of cases tumor was only detectable in the Smart MAR series. As well as Smart MAR, use of O-MAR or other comparable and projection-based MAR algorithm (SEMAR) allowed improved depiction of obscured structures in areas previously obscured by metal artifacts [24,25].

Unfortunately, as it was shown for other MAR techniques, artifacts persist directly adjacent to metal implants and severely degrade diagnostic image quality in these areas [12]. Although induction of new artifacts or underestimation of implant size was not evaluated in our study, no rater described complete failure of MAR software or considerable induction of new artifacts. As induction of new artifacts by MAR algorithms is a topic [2,4,19,24], this issue should be investigated further in future studies.

Comparison of our findings with recent results obtained with MAR algorithms for dual-source CT scans is difficult due to the fundamentally different technologies underlying artifact reduction. Nevertheless, some studies show a positive effect of iterative postprocessing also for DE-CT datasets [12]. Anyway, recent investigators see the future of MAR in combining DE-CT with state-of-the-art reconstruction algorithms [1].

As a post-processing algorithm, use of Smart MAR requires no additional radiation exposure, mean radiation dose of Smart MAR reconstructed CT datasets was comparatively low. For an ultra-low-dose scan of the head and neck region mean radiation dose was 7.27 ± 0.93 mGy per slice, which is approximately 32% higher than in our study [26]. No image transfer or manual processing was necessary after initial adjustments (pitch of 0.9), distinguishing Smart MAR from other MAR algorithms [19,27].

Some further limitations of the present work should be mentioned. First, as it was shown in other studies, different visual appearance of reconstructed series precludes full blinding and might have biased subjective rating. Second, we did not take the heterogeneous material of metal implants into account and rated only the extend of artifacts, what might have biased the results.

Interesting topics of further research might be the comparison of the Smart MAR with other promising MAR algorithms in single and dual source CT and use in CT for evaluation of orthopedic implants.

5. Conclusions

Even when heavy artifacts are present, the supplementary use of the Smart MAR post-processing tool seems to significantly improve both subjective and objective image quality as well as diagnostic confidence and lesion detection in CT of the head and neck. Tumor detection was 22% higher in Smart MAR reconstructed images.

Declaration of Competing Interest

The authors declare no potential conflicts of interest with respect to the research, authorship, and publication of this article. This research did not receive any specific grant from funding.

References

[1] L. Gjesteby, B. De Man, Y. Jin, H. Paganetti, J. Verburg, D. Giantsoudi, G. Wang, Metal Artifact Reduction in CT: Where Are We After Four Decades? IEEE Access (2016), https://doi.org/10.1109/ACCESS.2016.2608621.

[2] F.E. Boas, D. Fleischmann, Evaluation of two iterative techniques for reducing metal artifacts in computed tomography, Radiology 259 (2011) 894–902, https://doi.org/10.1148/radiol.11101782.

[3] M. Axente, A. Paidi, R. Von Eyben, C. Zeng, A. Bani-Hashemi, A. Krauss, D. Hristov, Clinical evaluation of the iterative metal artifact reduction algorithm for CT simulation in radiotherapy, Med. Phys. 42 (2015) 1170–1183, https://doi.org/10.1118/1.4906245.

[4] J.Y. Huang, J.R. Kerns, J.L. Nute, X. Liu, P. a Balter, F.C. Stingo, D.S. Followill, D. Mirkovic, R.M. Howell, S.F. Kry, An evaluation of three commercially available metal artifact reduction methods for CT imaging, Phys. Med. Biol. 60 (2015) 1047–1067, https://doi.org/10.1088/0031-9155/60/3/1047.

[5] K. Matsumoto, M. Jinzaki, Y. Tanami, A. Ueno, M. Yamada, S. Kuribayashi, Virtual monochromatic spectral imaging with fast kilovoltage switching: improved image quality as compared with that obtained with conventional 120-kVp CT, Radiology 259 (2011) 257–262, https://doi.org/10.1148/radiol.11100978.

[6] D. Zhang, X. Li, B. Liu, Objective characterization of GE discovery CT750 HD scanner: gemstone spectral imaging mode, Med. Phys. 38 (2011) 1178–1188, https://doi.org/10.1118/1.3551999.

[7] F. Bamberg, A. Dierks, K. Nikolaou, M.F. Reiser, C.R. Becker, T.R.C. Johnson, Metal artifact reduction by dual energy computed tomography using monoenergetic extrapolation, Eur. Radiol. 21 (2011) 1424–1429, https://doi.org/10.1007/s00330-011-2062-1.

[8] P.A. Gondim Teixeira, J.B. Meyer, C. Baumann, A. Raymond, F. Sirveaux, H. Coudane, A. Blum, total hip prosthesis CT with single-energy projection-based metallic artifact reduction: impact on the visualization of specific periprosthetic soft tissue structures, Skeletal Radiol. 43 (2014) 1237–1246, https://doi.org/10.1007/s00256-014-1923-5.

[9] M. Katsura, J. Sato, M. Akahane, A. Kunimatsu, O. Abe, Current and novel techniques for metal artifact reduction at CT: practical guide for radiologists, RadioGraphics. 38 (2018) 450–461, https://doi.org/10.1148/rg.2018170102.

[10] G. Healthcare, 3000 N. Grandview Blvd., W. 53188 Waukesha, U.S.A, Smart MAR White Paper, (n.d.).

[11] E. Shim, Y. Kang, J.M. Ahn, E. Lee, J.W. Lee, J.H. Oh, H.S. Kang, Metal artifact

reduction for orthopedic implants (O-MAR): usefulness in CT evaluation of reverse total shoulder arthroplasty, Am. J. Roentgenol. 209 (2017) 860–866, https://doi.org/10.2214/AJR.16.17684.
[12] J. Weiß, C. Schabel, M. Bongers, R. Raupach, S. Clasen, M. Notohamiprodjo, K. Nikolaou, F. Bamberg, Impact of iterative metal artifact reduction on diagnostic image quality in patients with dental hardware, Acta radiol. (2016), https://doi.org/10.1177/0284185116646144.
[13] M.L. Schäfer, L. Lüdemann, G. Böning, J. Kahn, S. Fuchs, B. Hamm, F. Streitparth, Radiation dose reduction in CT with adaptive statistical iterative reconstruction (ASIR) for patients with bronchial carcinoma and intrapulmonary metastases, Clin. Radiol. 71 (2016) 442–449, https://doi.org/10.1016/j.crad.2016.01.013.
[14] N. Desai, A. Singh, D.J. Valentino, Practical Evaluation of Image Quality in Computed Radiographic (CR) Imaging Systems 1 (2010), p. 76224Q, https://doi.org/10.1117/12.844640.
[15] G. Norman, Likert scales, levels of measurement and the “laws” of statistics, Adv. Health Sci. Educ. Theory Pract. (2010), https://doi.org/10.4025/dialogos.v20n2.34581.
[16] J.R. Landis, G.G. Koch, The measurement of observer agreement for categorical data, Biometrics. (1977), https://doi.org/10.2307/2529310.
[17] J.M. Bland, D.G. Altman, Statistics notes: multiple significance tests: the Bonferroni method, BMJ. (1995), https://doi.org/10.1136/bmj.310.6973.170.
[18] S. Jeong, S.H. Kim, E.J. Hwang, C.-I. Shin, J.K. Han, B.I. Choi, Usefulness of a metal artifact reduction algorithm for orthopedic implants in abdominal CT: phantom and clinical study results, AJR Am. J. Roentgenol. 204 (2015) 307–317, https://doi.org/10.2214/AJR.14.12745.
[19] H. Li, C. Noel, H. Chen, H. Harold Li, D. Low, K. Moore, P. Klahr, J. Michalski, H.A. Gay, W. Thorstad, S. Mutic, Clinical evaluation of a commercial orthopedic metal artifact reduction tool for CT simulations in radiation therapy, Med. Phys. 39 (2012) 7507–7517, https://doi.org/10.1118/1.4762814.
[20] G. Böning, M. Schäfer, U. Grupp, D. Kaul, J. Kahn, M. Pavel, M. Maurer, T. Denecke, B. Hamm, F. Streitparth, Comparison of applied dose and image quality in staging CT of neuroendocrine tumor patients using standard filtered back projection and adaptive statistical iterative reconstruction, Eur. J. Radiol. 84 (2015) 1601–1607, https://doi.org/10.1016/j.ejrad.2015.04.017.
[21] K. Miki, S. Mori, A. Hasegawa, K. Naganawa, M. Koto, Single-energy metal artefact reduction with CT for carbonion radiation therapy treatment planning, Br. J. Radiol. 89 (2016), https://doi.org/10.1259/bjr.20150988.
[22] K.M. Andersson, C.V. Dahlgren, J. Reizenstein, Y. Cao, A. Ahnesjö, P. Thunberg, Evaluation of two commercial CT metal artifact reduction algorithms for use in proton radiotherapy treatment planning in the head and neck area, Med. Phys. (2018), https://doi.org/10.1002/mp.13115.
[23] W. Wuest, M.S. May, M. Brand, N. Bayerl, A. Krauss, M. Uder, X.M. Lell, Improved image quality in head and neck ct using a 3d iterative approach to reduce metal artifact, Am. J. Neuroradiol. (2015), https://doi.org/10.3174/ajnr.A4386.
[24] M. Kidoh, T. Nakaura, S. Nakamura, S. Tokuyasu, H. Osakabe, K. Harada, Y. Yamashita, Reduction of dental metallic artefacts in CT: value of a newly developed algorithm for metal artefact reduction (O-MAR), Clin. Radiol. 69 (2014), https://doi.org/10.1016/j.crad.2013.08.008.
[25] K. Yasaka, K. Kamiya, R. Irie, E. Maeda, J. Sato, K. Ohtomo, Metal artefact reduction for patients with metallic dental fillings in helical neck computed tomography: comparison of adaptive iterative dose reduction 3D (AIDR 3D), forward-projected modelbased iterative reconstruction solution (FIRST) and AIDR 3D with, Dentomaxillofacial Radiol. 45 (2016) 1–7, https://doi.org/10.1259/dmfr.20160114.
[26] R. Gnannt, A. Winklehner, R. Goetti, B. Schmidt, S. Kollias, H. Alkadhi, Low kilovoltage CT of the neck with 70 kVp: comparison with a standard protocol, Am. J. Neuroradiol. 33 (2012) 1014–1019, https://doi.org/10.3174/ajnr.A2910.
[27] M.H. Albrecht, J.-E. Scholtz, J. Kraft, R.W. Bauer, M. Kaup, P. Dewes, A.M. Bucher, I. Burck, J. Wagenblast, T. Lehnert, J.M. Kerl, T.J. Vogl, J.L. Wichmann, Assessment of an Advanced Monoenergetic Reconstruction Technique in Dual-Energy Computed Tomography of Head and Neck Cancer, Eur. Radiol. 25 (2015) 2493–2501, https://doi.org/10.1007/s00330-015-3627-1.